Available online at www.sciencedirect.com
SCIENCE DIRECT®
International Journal of Heat and Mass Transfer 47 (2004) 4293–4300
International Journal of HEAT and MASS TRANSFER
www.elsevier.com/locate/ijhmt

An analytical derivation of source term dependent, 2-D 'generalized Poisson conduction shape factors'

Devashish Shrivastava, Robert B. Roemer *

Department of Mechanical Engineering, University of Utah, Salt Lake City, UT 84102, USA

Received 30 September 2003; received in revised form 26 April 2004
Available online 2 July 2004

Abstract

This paper presents derivations for new "generalized Poisson conduction shape factors" (GPCSFs), that are more general than the commonly used conduction shape factors since they include the effects of both source terms and arbitrary, spatially variable boundary temperatures. The GPCSFs are derived for a single, circular vessel eccentrically imbedded in a uniformly heated, homogeneous, circular tissue matrix. Two GPCSF formulations are presented, as based on the difference between the average vessel wall temperature and; (1) the average tissue boundary temperature (S_{tb}), or (2) the average tissue matrix temperature (S_{tm}). The results show first, that the presence of a source term significantly affects the GPCSFs for all vessel radii and eccentricities. Second, unlike standard shape factors with uniform boundary temperatures, the GPCSFs are a function of both the magnitude and distribution of the boundary temperatures; however, these effects are significant only for large vessel radii and eccentricities. Finally, when the vessel cools the tissue, the average tissue matrix temperature GPCSFs are much less sensitive to the source term than are the tissue boundary temperature GPCSFs.

1. Introduction

To accurately estimate heat transfer rates between tissues and vessels in biological/medical applications, it is important to quantify convective and conductive resistances accurately. Since the conductive resistance dominates or is at least comparable to the convective resistance in tissue–vessel heat transfer [e.g., 1], previous investigators have focused on developing improved conduction shape factors [e.g., 1–6] by using several different approximations and formulations. First, in many applications strong source terms are present in the tissue, surprisingly, no expressions have been derived for the related shape factors. Thus, previous investigators have approximated them using shape factors derived using Laplace's equation [e.g., 2,4]. More particularly, the development of new, more robust equations to predict tissue temperatures, e.g., the tissue convective energy balance equation, TCEBE [7], requires knowledge of shape factors for heated tissues, thus specifically motivating the current study.

Second, (again surprisingly) all previous investigators have used only uniform boundary conditions [3,5,6, 8–12] to derive shape factors. However, variable boundary conditions will clearly be present on vessel surfaces due to the non-uniform temperature distributions in unheated/heated tissues. Thus, it is important to derive GPCSFs using angularly varying boundary conditions to determine the effect of these variables.

Third, there are several different ways in which conduction "shape factors" have been defined in the biothermal literature. Some researchers have based them on the difference between the vessel wall and tissue boundary temperatures [e.g., 1–3]. Alternatively, Baish et al. [4] (implicitly) defined them based on the difference between the vessel wall temperature and the volume

* Corresponding author. Tel.: +1-801-585-5631; fax: +1-801-585-9826.
E-mail address: bob.roemer@utah.edu (R.B. Roemer).

0017-9310/$ - see front matter © 2004 Elsevier Ltd. All rights reserved.
doi:10.1016/j.ijheatmasstransfer.2004.04.027

Nomenclature

a_{vw}	dimensional distance between the centers of the tissue and the vessel
f_{vw}	an arbitrary temperature function at the boundary of the vessel
f_{tb}	an arbitrary temperature function at the outer boundary of the tissue
g'''	uniform source term in the tissue per unit volume
k	conductivity of the tissue
r	radial distance
r_{vw}	radius of the vessel
r_{tb}	outer radius of the cylinder
S_{tb}	generalized Poisson conduction shape factor defined based on the average tissue boundary temperature
S_{tm}	generalized Poisson conduction shape factor defined based on the area average tissue matrix temperature
$t_{tb,1}$	average temperature at the outer tissue boundary
$t_{tb,2}$	magnitude of the temperature fluctuation imposed on the tissue outer wall
$t_{vw,1}$	average temperature at the vessel wall
$t_{vw,2}$	magnitude of the temperature fluctuation imposed on the vessel wall

Non-dimensional parameters

A_{vw}	distance between the center of the tissue and the center of the vessel, a_{vw}/r_{tb}
a_{11}	constant, $A_{vw} - R_{vw}$
a_{21}	constant, $A_{vw} + R_{vw}$
F_{tb}	temperature at the tissue boundary, $(f_{tb} - t_{vw,1})/(t_{tb,1} - t_{vw,1})$
F_{vw}	temperature at the vessel wall, $(f_{vw} - t_{vw,1})/(t_{tb,1} - t_{vw,1})$
n_{tb}	constant that determines the number of peaks in the temperature fluctuation on the tissue boundary
n_{vw}	constant that determines the number of peaks in the temperature fluctuation on the vessel wall
P	power deposition, $g''' r_{tb}^2 k/(t_{tb,1} - t_{vw,1})$
R	radius, r/r_{tb}
R_1	distance of the vessel wall perimeter from the center of the tissue matrix, $\{(A_{vw} + R_{vw}\cos\theta)^2 + (R_{vw}\sin\theta)^2\}^{1/2}$
R_1^*	radius in conformally mapped space, $(U_1^2 + V_1^2)^{1/2}$
R_m	radius of the vessel in conformally mapped space, $\{1 - a_{11}a_{21} - ((1 - a_{11}^2)(1 - a_{21}^2))^{1/2}\}/(a_{21} - a_{11})$
R_{vw}	radius of the vessel, r_{vw}/r_{tb}
T	temperature, $(t - t_{vw,1})/(t_{tb,1} - t_{vw,1})$
T_1	temperature, $T + PR^2/4$
T_{avg}	area average non-dimensional temperature of the tissue matrix, $\frac{1}{A}\int_A T\,dA$
U_1, V_1	Cartesian coordinate system in the conformal plane
w_1	bilinear transformation, $U_1 + iV_1 = (x + iy - \lambda_1)/(1 - \lambda_1(x + iy))$
x, y	original Cartesian coordinate system

Greek symbols

α_1	angular position measured from the center of the vessel in the transformed coordinate system, $\tan^{-1}(V_1/U_1)$
λ_1	constant, $\{1 + a_{11}a_{21} - ((1 - a_{11}^2)(1 - a_{21}^2))^{1/2}\}/(a_{21} + a_{11})$
ϕ_{tb}	phase angle of the temperature fluctuation at the tissue boundary
ϕ_{vw}	phase angle of the temperature fluctuation at the vessel wall
ψ	angular position measured from the center of the disk
θ	angular position measured from the center of the vessel in the original coordinate system

averaged tissue temperature. Finally, others have defined such factors based on the difference between the mixed mean blood temperature and (1) the temperature outside the boundary [e.g., 5,6,8] or (2) on the tissue boundary [e.g., 9].

In summary, a derivation for shape factors that are valid for general vessel wall and tissue boundary conditions is needed for both heated/unheated tissues. The current derivation derives such expressions for a single vessel in a finite tissue matrix. Derivations for multiple vessels will be presented in future publications [13].

2. Mathematical model

2.1. Formulation and solution

To derive the new GPCSFs we solve the 2-D energy equation with a uniformly distributed source term for a single circular vessel eccentrically imbedded in a circular tissue matrix. General Dirichlet boundary conditions are utilized. A uniform source distribution is assumed: (a) for simplicity, and (b) since the source term distribution for many heating systems whose power deposition patterns vary negligibly over distances of the magnitude of

the tissue boundary radius can be approximated as being uniform over short distances. A single vessel is used since it has been shown by Xu et al. [14] that if the tissue matrix area is on the order of 1 mm^2 the vessel number density ranges from 1 to 3 vessels/mm^2 in a pig kidney. The non-dimensional energy equation is presented in Eq. (1) after the change of variables from T to T_1 to make this equation a Laplace equation for a homogeneous tissue matrix with an arbitrarily located vessel. Boundary conditions are given in Eqs. (2) and (3) (Fig. 1).

$$\frac{1}{R}\frac{\mathrm{d}}{\mathrm{d}R}\left(R\frac{\mathrm{d}T_1}{\mathrm{d}R}\right)+\frac{1}{R^2}\frac{\mathrm{d}^2T_1}{\mathrm{d}\psi^2}=0 \tag{1}$$

$$T_1|_{R_1}=F_{\mathrm{vw}}(\theta)+PR_1/4 \tag{2}$$

$$T_1|_1=F_{\mathrm{tb}}(\psi)+P/4 \tag{3}$$

A bilinear transformation (w_1) [15] is applied to make the tissue and vessel cylinders concentric, giving,

$$\frac{1}{R_1^*}\frac{\mathrm{d}}{\mathrm{d}R_1^*}\left(R_1^*\frac{\mathrm{d}T_1}{\mathrm{d}R_1^*}\right)+\frac{1}{(R_1^*)^2}\frac{\mathrm{d}^2T_1}{\mathrm{d}\alpha_1^2}=0 \tag{4}$$

with,

$$T_1|_1=F_{\mathrm{tb}}(\psi(U_1,V_1))+P/4 \tag{5}$$

$$T_1|_{R_{\mathrm{m}}}=F_{\mathrm{vw}}(\theta(U_1,V_1))+PR_1(U_1,V_1)^2/4 \tag{6}$$

The general solution to Eq. (4) is [16],

$$T_1=A_{01}+A'_{01}\ln(R_1^*)+\sum_{n=1}^{\infty}\{A_{n1}(R_1^*)^n+A'_{n1}(R_1^*)^{-n}\}\times\sin(n\alpha_1)+\sum_{n=1}^{\infty}\{B_{n1}(R_1^*)^n+B'_{n1}(R_1^*)^{-n}\}\cos(n\alpha_1) \tag{7}$$

Using Eqs. (5) and (6) and orthogonality gives,

$$A_{01}=\frac{1}{2\pi}\int_0^{2\pi}F_{\mathrm{tb}}(\psi(U_1,V_1))\,\mathrm{d}\alpha_1+P/4 \tag{8}$$

$$A'_{01}=\frac{1}{\log(R_{\mathrm{m}})}\left[\frac{1}{2\pi}\int_0^{2\pi}\left(F_{\mathrm{vw}}(\theta(U_1,V_1))+\frac{PR_1(U_1,V_1)^2}{4}\right)\mathrm{d}\alpha_1-A_0\right] \tag{9}$$

$$A_{n1}+A'_{n1}=S_{\mathrm{A}_{n1}}=\frac{1}{\pi}\int_0^{2\pi}F_{\mathrm{tb}}(\psi(U_1,V_1))\sin(n\alpha_1)\,\mathrm{d}\alpha_1 \tag{10}$$

$$B_{n1}+B'_{n1}=S_{\mathrm{B}_{n1}}=\frac{1}{\pi}\int_0^{2\pi}F_{\mathrm{tb}}(\psi(U_1,V_1))\cos(n\alpha_1)\,\mathrm{d}\alpha_1 \tag{11}$$

$$A_{n1}=\frac{1}{(R_{\mathrm{m}}^n-R_{\mathrm{m}}^{-n})}\left[\frac{1}{\pi}\int_0^{2\pi}\left(F_{\mathrm{vw}}(\theta(U_1,V_1))+\frac{PR_1(U_1,V_1)^2}{4}\right)\sin(n\alpha_1)\,\mathrm{d}\alpha_1-S_{\mathrm{A}_{n1}}R_{\mathrm{m}}^{-n}\right] \tag{12}$$

$$B_{n1}=\frac{1}{(R_{\mathrm{m}}^n-R_{\mathrm{m}}^{-n})}\left[\frac{1}{\pi}\int_0^{2\pi}\left(F_{\mathrm{vw}}(\theta(U_1,V_1))+\frac{PR_1(U_1,V_1)^2}{4}\right)\times\cos(n\alpha_1)\,\mathrm{d}\alpha_1-S_{\mathrm{B}_{n1}}R_{\mathrm{m}}^{-n}\right] \tag{13}$$

Eqs. (7)–(13) describe the temperature field in the tissue. This solution is valid for any continuous vessel wall and

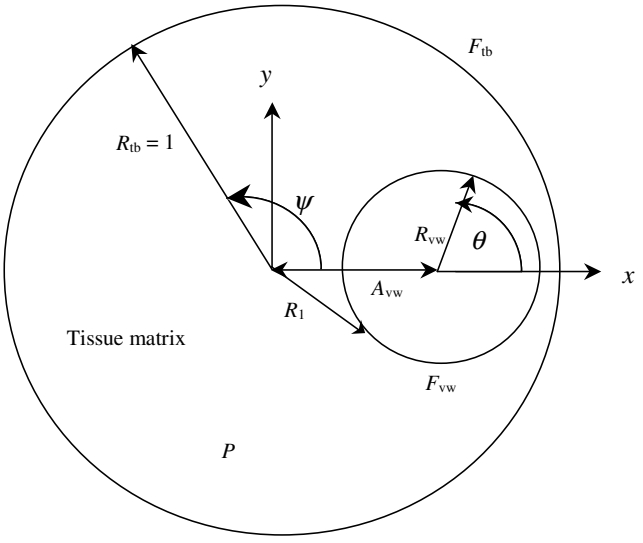

Fig. 1. Schematic of an arbitrarily located vessel inside a tissue matrix.

tissue boundary temperature fields that can be represented by a Fourier series, and reduces to the standard solutions under proper conditions [13].

The two GPCSFs are now defined. First, Eq. (14) defines the GPCSF S_{tb} as the heat transfer rate from the tissue to the vessel divided by the difference between the average tissue boundary and vessel wall temperatures. Eq. (14) is a generalized extension of the conventional shape factor since it reduces to it [17] for no source term and uniform boundary temperatures.

$$\frac{S_{tb}}{L} = \int_0^{2\pi} R_{vw} \left.\frac{dT}{dR}\right|_{R=R_{vw}} d\theta \tag{14}$$

Second, Eq. (15) defines S_{tm} as the heat transfer rate from the tissue to the vessel divided by the difference between the average tissue matrix and vessel wall temperatures,

$$\frac{S_{tm}}{L} = \frac{\int_0^{2\pi} R_{vw} \left.\frac{dT}{dR}\right|_{R=R_{vw}} d\theta}{T_{avg}} \tag{15}$$

2.2. Parametric solutions

To study the effect of the boundary conditions for a case of biological interest, Eqs. (16) and (17) are used since Wissler [18] has shown that for two nearby vessels, the angular variations in vessel wall temperatures are similar to a cosine function.

$$\begin{aligned} F_{vw}(\theta) &= 0 + \frac{t_{vw,2}}{t_{tb,1} - t_{vw,1}} \cos(n_{vw}\theta + \phi_{vw}) \\ &= 0 + T_{vw,2} \cos(n_{vw}\theta + \phi_{vw}) \end{aligned} \tag{16}$$

$$\begin{aligned} F_{tb}(\psi) &= 1 + \frac{t_{tb,2}}{t_{tb,1} - t_{vw,1}} \cos(n_{tb}\psi + \phi_{tb}) \\ &= 1 + T_{tb,2} \cos(n_{tb}\psi + \phi_{tb}) \end{aligned} \tag{17}$$

In Eqs. (16) and (17), $T_{vw,2}$ and $T_{tb,2}$ are negative when the average vessel wall temperature is higher than the average tissue boundary temperature, i.e. the vessel heats the tissue. Boundary condition effects are studied by: (1) giving different values to the magnitudes of the fluctuations ($t_{vw,2}$ and $t_{tb,2}$); (2) rotating the imposed temperature fields between 0 and 2π by changing phase angles (ϕ_{vw} and ϕ_{tb}) and; (3) varying the number of fluctuation peaks by changing n_{vw} and n_{tb}. The effects of vessel wall temperature fluctuation magnitude ($t_{vw,2}$) are studied for the magnitudes of $T_{vw,2} = 0$, 0.5 and 1, with the fixed tissue boundary temperature fluctuation value ($T_{tb,2}$) of 1. This simulates actual vessel wall temperature fluctuations of the magnitudes of ± 0, 2.5 and 5 °C respectively, for the tissue boundary temperature fluctuation magnitudes of ±5 °C. These conditions correspond to therapeutic applications where the average vessel wall and the tissue boundary temperatures are 38 and 43 °C respectively [19–22].

The source term P is positive when the average tissue boundary temperature is higher than the average vessel wall temperature, and vice versa. The maximum value for P is chosen as 10 to study a typical thermal therapy application (i.e., when the difference between the average tissue matrix temperature and the average vessel wall temperature reaches approximately twice the difference between the average tissue boundary and vessel wall temperatures), and the vessel cools the tissue [19–22]. Similarly, to simulate conditions when the vessel heats the tissue, the minimum value of P is chosen as −7.5.

Although the effects of boundary conditions and source term can be modeled separately due to the problem's linearity, the effects of both of these variables are studied together. This is because both are present in typical therapeutic applications [19–22], and it allows us to directly compare their effects in a single paper.

3. Results

All results are given in non-dimensional form. Figs. 2 and 3 present the variation in S_{tb} and S_{tm} with vessel radius as a function of the magnitude of the source term and the vessel wall temperature fluctuations, for a given vessel eccentricity. Since vessels of ~50–1000 μm are thermally significant [3,17], the non-dimensional vessel radius, R_{vw} is varied from 0.025 to 0.50 using a tissue matrix radius of ~O(1 mm). The eccentricity A_{vw} is chosen as 0.4 to put part of the perimeter of the (large) vessel of the size $R_{vw} = 0.5$ close to the tissue boundary. Since n_{vw} and $n_{tb} = 1$, and ϕ_{vw} and $\phi_{tb} = 0$, the maximum vessel wall and tissue boundary temperatures are at $\theta = \psi = 0$, and the minima are at $\theta = \psi = \pi$.

Figs. 4 and 5 present the variation in S_{tb} and S_{tm} with vessel eccentricity as a function of the magnitude of the source term and the vessel wall temperature fluctuation, for a vessel radius of 0.25.

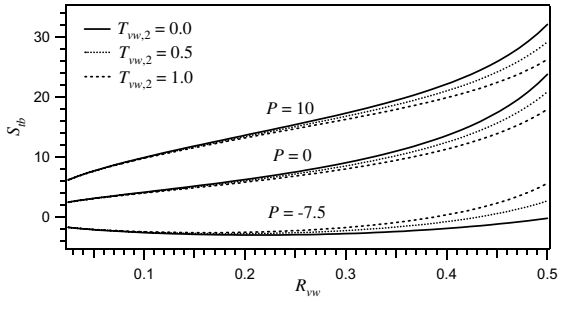

Fig. 2. S_{tb} vs R_{vw} for $A_{vw} = 0.4$, $T_{tb,2} = 1.0$, $n_{vw} = n_{tb} = 1$, and $\phi_{vw} = \phi_{tb} = 0$. When $P = 0$ and 10, $t_{tb,1} - t_{vw,1} = 5.0$ °C, and when $P = -7.5$, $t_{tb,1} - t_{vw,1} = -5.0$ °C.

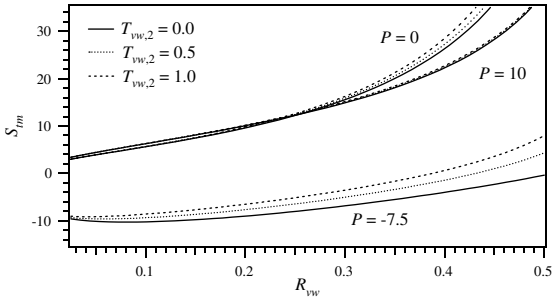

Fig. 3. S_{tm} vs R_{vw} for $A_{\mathrm{vw}} = 0.4$, $T_{\mathrm{tb},2} = 1.0$, $n_{\mathrm{vw}} = n_{\mathrm{tb}} = 1$, and $\phi_{\mathrm{vw}} = \phi_{\mathrm{tb}} = 0$. When $P = 0$ and 10, $t_{\mathrm{tb},1} - t_{\mathrm{vw},1} = 5.0$ °C, and when $P = -7.5$, $t_{\mathrm{tb},1} - t_{\mathrm{vw},1} = -5.0$ °C.

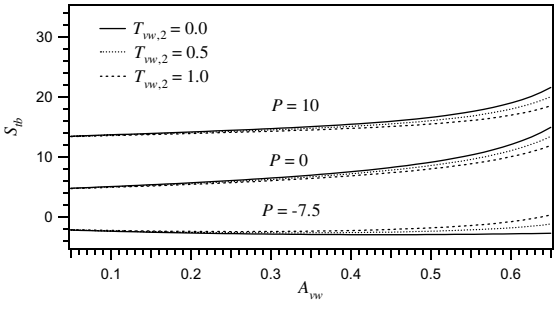

Fig. 4. S_{tb} vs A_{vw} for $R_{\mathrm{vw}} = 0.25$, $T_{\mathrm{tb},2} = 1.0$, $n_{\mathrm{vw}} = n_{\mathrm{tb}} = 1$, and $\phi_{\mathrm{vw}} = \phi_{\mathrm{tb}} = 0$. When $P = 0$ and 10, $t_{\mathrm{tb},1} - t_{\mathrm{vw},1} = 5.0$ °C, and when $P = -7.5$, $t_{\mathrm{tb},1} - t_{\mathrm{vw},1} = -5.0$ °C.

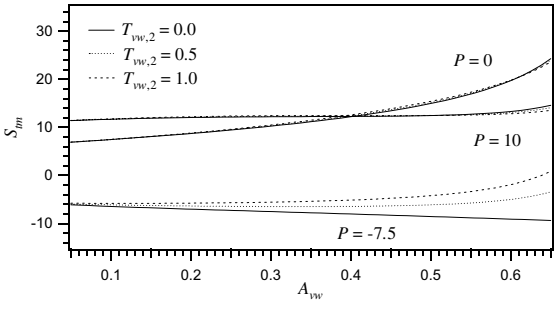

Fig. 5. S_{tm} vs A_{vw} for $R_{\mathrm{vw}} = 0.25$, $T_{\mathrm{tb},2} = 1.0$, $n_{\mathrm{vw}} = n_{\mathrm{tb}} = 1$, and $\phi_{\mathrm{vw}} = \phi_{\mathrm{tb}} = 0$. When $P = 0$ and 10, $t_{\mathrm{tb},1} - t_{\mathrm{vw},1} = 5.0$ °C, and when $P = -7.5$, $t_{\mathrm{tb},1} - t_{\mathrm{vw},1} = -5.0$ °C.

Fig. 6 presents the effect of the phase angles ϕ_{tb} and ϕ_{vw} on S_{tb} for a small vessel, at both a small and a large vessel eccentricity, for three vessel wall temperature fluctuation and source term magnitudes. Fig. 7 presents the effect of the phase angles ϕ_{tb} and ϕ_{vw} on S_{tb} at a small vessel eccentricity for both a small and a large vessel radius, for the same vessel wall temperature fluctuations and source terms as in Fig. 6. (The comparable

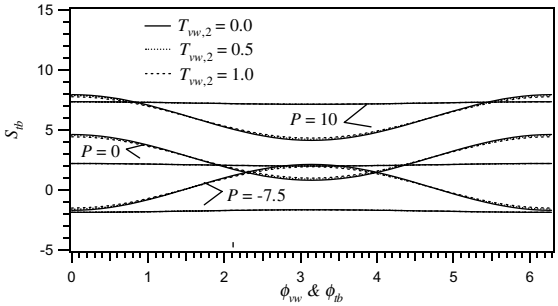

Fig. 6. S_{tb} vs $\phi_{\mathrm{vw}} = \phi_{\mathrm{tb}}$ for $A_{\mathrm{vw}} = 0.05$ and 0.70, $R_{\mathrm{vw}} = 0.05$, $T_{\mathrm{tb},2} = 1.0$, and $n_{\mathrm{vw}} = n_{\mathrm{tb}} = 1$. When $P = 0$ and 10, $t_{\mathrm{tb},1} - t_{\mathrm{vw},1} = 5.0$ °C, and when $P = -7.5$, $t_{\mathrm{tb},1} - t_{\mathrm{vw},1} = -5.0$ °C. Straight lines are for $A_{\mathrm{vw}} = 0.05$ and curved lines are for $A_{\mathrm{vw}} = 0.70$.

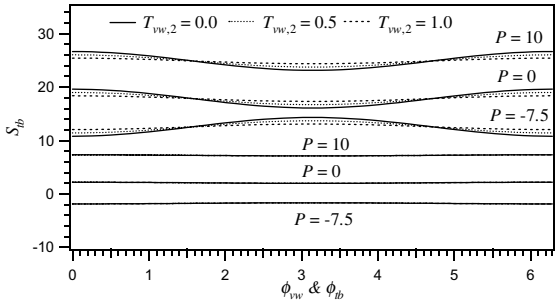

Fig. 7. S_{tb} vs $\phi_{\mathrm{vw}} = \phi_{\mathrm{tb}}$ for $A_{\mathrm{vw}} = 0.05$, $R_{\mathrm{vw}} = 0.05$ and 0.70, $T_{\mathrm{tb},2} = 1.0$, and $n_{\mathrm{vw}} = n_{\mathrm{tb}} = 1$. When $P = 0$ and 10, $t_{\mathrm{tb},1} - t_{\mathrm{vw},1} = 5.0$ °C, and when $P = -7.5$, $t_{\mathrm{tb},1} - t_{\mathrm{vw},1} = -5.0$ °C. Straight lines are for $R_{\mathrm{vw}} = 0.05$ and curved lines are for $R_{\mathrm{vw}} = 0.70$.

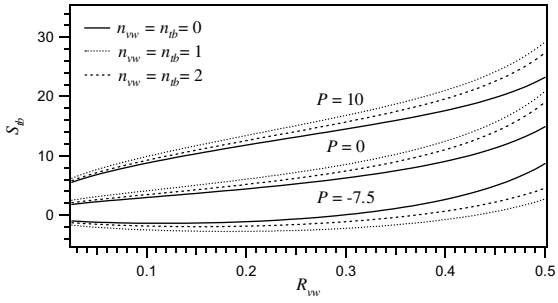

Fig. 8. S_{tb} vs R_{vw} for $A_{\mathrm{vw}} = 0.4$, and $\phi_{\mathrm{vw}} = \phi_{\mathrm{tb}} = 0$. When $n_{\mathrm{vw}} = n_{\mathrm{tb}} = 0$, $T_{\mathrm{vw},2} = T_{\mathrm{tb},2} = 0$, and when $n_{\mathrm{vw}} = n_{\mathrm{tb}} > 0$, $T_{\mathrm{vw},2} = 0.5$, $T_{\mathrm{tb},2} = 1.0$. When $P = 0$ and 10, $t_{\mathrm{tb},1} - t_{\mathrm{vw},1} = 5.0$ °C, and when $P = -7.5$, $t_{\mathrm{tb},1} - t_{\mathrm{vw},1} = -5.0$ °C.

S_{tm} cases are not shown since the results are similar to those for S_{tb}.)

Fig. 8 presents the variation in S_{tb} vs. vessel radius as a function of the strength of the source term and the frequency of the vessel wall temperature fluctuations, for

a given vessel eccentricity. The R_{vw} and A_{vw} values are as in Fig. 2. Results are presented for $n_{vw} = n_{tb} = 0$, 1, and 2 for cases when the vessel cools the tissue and vice versa. To keep the average vessel wall and tissue boundary temperatures the same for all n_{vw} values, the magnitudes of the vessel wall and tissue boundary temperature fluctuations are set to zero for $n_{vw} = n_{tb} = 0$ (Figs. 8–11).

To compare the S_{tb} results in Fig. 8 with the comparable S_{tm} results, Fig. 9 shows S_{tm} as a function of the vessel radius for a given vessel eccentricity as a function of the strength of the source term and the frequency of the vessel wall temperature fluctuations. The R_{vw} and the A_{vw} values are as in Fig. 2. Results are presented for $n_{vw} = n_{tb} = 0$ and 1 when the vessel cools the tissue, and for $n_{vw} = n_{tb} = 0$, 1, and 2 when the vessel heats the tissue (Figs. 9 and 11).

Finally, Figs. 10 and 11 present the variation in S_{tb} and S_{tm} vs. vessel eccentricity for a given vessel radius as a function of the frequency of the vessel wall temperature fluctuations for three source term strengths. The R_{vw} and A_{vw} values are as in Fig. 4.

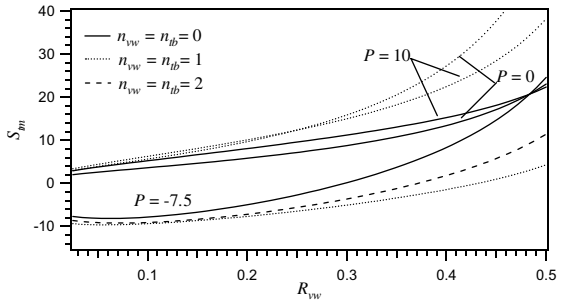

Fig. 9. S_{tm} vs R_{vw} for $A_{vw} = 0.4$, and $\phi_{vw} = \phi_{tb} = 0$. When $n_{vw} = n_{tb} = 0$, $T_{vw,2} = T_{tb,2} = 0$, and when $n_{vw} = n_{tb} > 0$, $T_{vw,2} = 0.5$, $T_{tb,2} = 1.0$. When $P = 0$ and 10, $t_{tb,1} - t_{vw,1} = 5.0$ °C, and when $P = -7.5$, $t_{tb,1} - t_{vw,1} = -5.0$ °C.

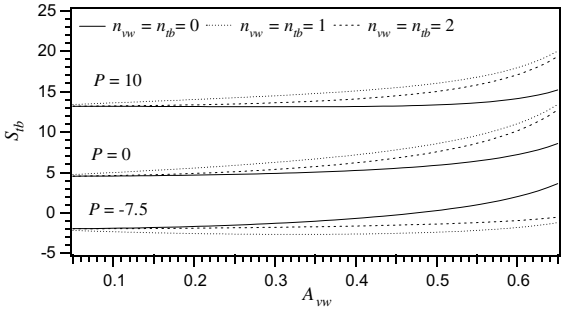

Fig. 10. S_{tb} vs A_{vw} for $R_{vw} = 0.25$, and $\phi_{vw} = \phi_{tb} = 0$. When $n_{vw} = n_{tb} = 0$, $T_{vw,2} = T_{tb,2} = 0$, and when $n_{vw} = n_{tb} > 0$, $T_{vw,2} = 0.5$, $T_{tb,2} = 1.0$. When $P = 0$ and 10, $t_{tb,1} - t_{vw,1} = 5.0$ °C, and when $P = -7.5$, $t_{tb,1} - t_{vw,1} = -5.0$ °C.

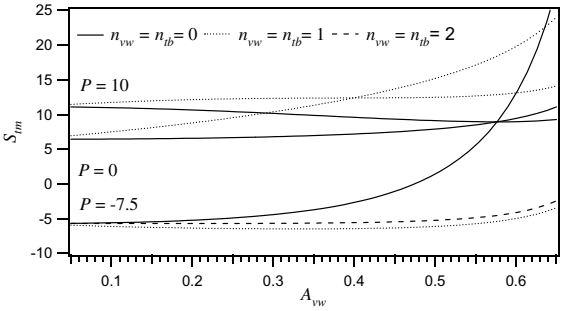

Fig. 11. S_{tm} vs A_{vw} for $R_{vw} = 0.25$, and $\phi_{vw} = \phi_{tb} = 0$. When $n_{vw} = n_{tb} = 0$, $T_{vw,2} = T_{tb,2} = 0$, and when $n_{vw} = n_{tb} > 0$, $T_{vw,2} = 0.5$, $T_{tb,2} = 1.0$. When $P = 0$ and 10, $t_{tb,1} - t_{vw,1} = 5.0$ °C, and when $P = -7.5$, $t_{tb,1} - t_{vw,1} = -5.0$ °C.

4. Discussion

First, Figs. 2, 4, 6–8 and 10 show that power deposition affects S_{tb} significantly for all conditions. This dependency arises since an increase in power increases the net energy inflow into the vessel—and thus the value of S_{tb}—while both the vessel wall and the tissue boundary temperatures are fixed. Thus, the use of conventional shape factors in cases where heating is present can introduce significant errors.

Conversely, the S_{tm} values are not nearly as affected by the power magnitude when the vessel cools the tissue (Figs. 3, 5, 9 and 11). This result is explained since as P increases, not only does the heat flux into the vessel increase, but so does the average tissue matrix temperature—and thus the difference between the average tissue matrix temperature and the (fixed) average vessel wall temperature also increases. In summary the use of S_{tm} instead of S_{tb} is recommended when the blood cools the tissue.

On the other hand, as with S_{tb}, the values of S_{tm}, are strongly dependent on the power deposition magnitude when the average vessel wall temperature is higher than the average tissue boundary temperature ($P < 0$) (Figs. 3, 5, 9 and 11) for low power magnitudes. This significant dependency occurs since an increase in P increases both the heat flux into the vessel and the average tissue matrix temperature. This temperature then approaches the (fixed) average vessel wall temperature and their difference decreases, eventually reaching a singular point. Further increases in the magnitude of P increase both the inflow of energy to the vessel and the magnitude of the average tissue matrix temperature, and thus also their difference. Therefore, the S_{tm} curves for large, negative P values will be close together and closer to the

curves for $P > 0$ (not shown in Figs. 3, 5, 9 and 11) [13]. In summary, since both shape factors are dependent on both the applied power and the tissue temperature distribution (which is itself dependent on the applied power), iterative procedures are needed to solve for the 3-D tissue temperature field if either S_{tm} or S_{tb} is used to estimate the tissue–vessel heat transfer rates.

Second, Figs. 2–7 show that the effect of the vessel wall temperature fluctuation magnitude on the GPCSFs is significant only at large vessel radii/eccentricities. This occurs since for zero eccentricity, as the magnitude of the fluctuations increases everywhere (both +/−), any decrease in the heat flux from one part of the vessel is compensated for by an increase from another. However, as the vessel eccentricity increases, part of the vessel's perimeter comes closer to the tissue boundary when compared to the rest of the perimeter. Thus, for all other factors equal, this closer part becomes thermally more significant since the various parts of the vessel perimeter act as parallel resistances. Therefore for an eccentric vessel, as the fluctuation magnitude increases, an increase in the heat flux inflow to the vessel from one part of the vessel will not compensate the decrease in the heat flux elsewhere; i.e., the net increase/decrease in the inflow of the heat flux is determined more significantly by that part of the vessel closest to the tissue boundary (the "short circuit" effect). In particular for Figs. 2–5, the phase angles (ϕ_{vw} and ϕ_{tb}) are zero, $n_{vw} = n_{tb} = 1$ and the vessel eccentricity A_{vw} is positive, so an increase in the magnitude of the vessel wall fluctuation results in a net decrease in inflow of energy to the vessel from the tissue. This effect is more pronounced at high eccentricities and high vessel radii. The opposite curvatures of the $P > 0$ and $P < 0$ results arise when positive eccentricities are present, since when the vessel wall temperature is lower than the tissue boundary temperature ($P > 0$), an increase in the magnitude of the fluctuation in the average vessel wall temperature decreases the value of the GPCSFs and vice versa. In summary, the effect of the vessel wall fluctuation is present for all finite eccentricities, but is only significant at large eccentricities and radii.

Third, the GPCSFs are more sensitive to the vessel radius than to the eccentricity for all conditions (Figs. 2–11) since an increase in the vessel radius brings the whole vessel perimeter closer to the tissue boundary compared to an increase in the vessel eccentricity, which moves part of the perimeter closer to the tissue and the rest further away. This emphasizes the importance of knowing vessel radii compared to eccentricities.

Fourth, an increase in the frequency of the vessel wall temperature fluctuations affects S_{tm} (Figs. 9 and 11) more than S_{tb} (Figs. 8 and 10). For the case of the vessel cooling the tissue ($P > 0$), when the value of $n_{vw} = n_{tb}$ goes from 0 to 1, the local temperature difference between the vessel wall and tissue boundary increases in the "short circuit" part of the vessel perimeter and decreases in the rest of the vessel perimeter, thereby increasing the net tissue–vessel heat transfer rate and therefore the S_{tb}. The increased effect on S_{tm} arises since not only does the heat transfer rate increase as per the above "short circuit" argument, but on the opposite side of the vessel the overall local vessel wall and tissue boundary temperatures decrease, thereby decreasing the average tissue matrix temperature and thus increasing the S_{tm} more significantly than for S_{tb}. The opposite results for the case when the vessel heats the tissue can be explained similarly. As the values of $n_{vw} = n_{tb}$ increase to large values, the peaks and the troughs of the temperature fluctuations come closer together, thus increasing the heat transfer rates in the angular direction—and thereby canceling out each other's effects on both the tissue–vessel heat transfer rate and on the overall tissue temperature distribution. In the high frequency limit the shape factors approach those for the average tissue matrix temperature with no fluctuations on the vessel wall and tissue boundary ($n_{vw} = n_{tb} = 0$). This explains why curves for the GPCSFs for $n_{vw} = n_{tb} > 1$ are bounded by the curves for $n_{vw} = n_{tb}$ equal to 0 and 1 (Figs. 8–11).

An implication of these results is that it is important to model the frequency of the fluctuations in order to accurately model in vivo tissue–vessel heat transfer rates, and thus to accurately predict the in vivo temperature distributions. This, in a sense, is not an encouraging result, since it is very hard to estimate the frequency of the fluctuations on each of the vessel walls present in in vivo tissue where the temperature distribution, itself, is unknown. Fortunately, however, since all of the curves for GPCSFs for $n_{vw} = n_{tb} > 1$ are bounded by the curves for $n_{vw} = n_{tb}$ equal to 0 and 1, we can determine error estimates in calculating the GPCSFs and thus the tissue–vessel heat transfer rates.

Fifth, the effect of the phase angles ϕ_{vw} and ϕ_{tb} on the GPCSFs is significant for large radii and eccentricities (Figs. 6 and 7). This dependency can be explained since at high vessel radii and eccentricities, changes in the local temperature difference between the vessel wall and tissue boundary significantly affect the tissue–vessel heat transfer rate as well as the average tissue matrix temperature (refer to explanation above). This emphasizes the need to accurately model phase angles at high vessel radii and eccentricities to accurately estimate the tissue–vessel heat transfer rate and thus the tissue temperature distribution, which are seldom known. However, like the previous results, since it has been found that the GPCSFs are maximal when the difference in local vessel wall and tissue boundary temperatures in the thermally significant part of the vessel is a maximum and vice versa, error bounds can be estimated.

Sixth, using Figs. 2–11 it can be shown that the conductive resistance dominates or is equal to the convective resistance [1,23] for the power levels in the

present study. This motivates the extension of the present derivation to include multiple vessels [13].

5. Conclusions

New expressions for conduction shape factors have been derived that include the effects of uniform power deposition and variable temperature boundary conditions. Results show that when the average temperature of the vessel wall is lower than the average temperature of the tissue boundary, the GPCSFs based on the average tissue matrix temperature (S_{tm}) are much less sensitive to the strength of the source term compared to the GPCSFs based on the average tissue boundary temperature (S_{tb}). This result suggests that the use of S_{tm} instead of S_{tb} will introduce less error in the estimation of tissue–vessel heat transfer rates when sources are present. Finally, the effects of the variable vessel wall and tissue boundary temperatures are found to be significant at large vessel sizes and eccentricities, with vessel size having a larger effect than vessel eccentricity.

References

[1] M.M. Chen, K.R. Holmes, Microvascular contributions in tissue heat transfer, Ann. N.Y. Acad. Sci. 335 (1980) 137–150.
[2] J.J.W. Lagendijk, The influence of blood flow in large vessels on the temperature distribution in hyperthermia, Phys. Med. Biol. 27 (1) (1982) 17–23.
[3] J.C. Chato, Heat transfer to blood vessels, J. Biomech. Eng. 102 (1980) 110–118.
[4] J.W. Baish, P.S. Ayyaswamy, K.R. Foster, Small-scale temperature fluctuations in perfused tissue during local hyperthermia, J. Biomech. Eng. 108 (1986) 246–250.
[5] Y.L. Wu, S. Weinbaum, L.M. Jiji, A new analytic technique for 3-D heat transfer from a cylinder with two or more axially interacting eccentrically embedded vessels with application to countercurrent blood flow, Int. J. Heat Mass Transfer 36 (4) (1993) 1073–1083.
[6] L. Zhu, S. Weinbaum, A model for heat transfer from embedded blood vessels in 2-D tissue preparations, J. Biomech. Eng. 117 (1995) 64–73.
[7] R.B. Roemer, A.W. Dutton, A generic tissue convective energy balance equation: part 1—theory and derivation, J. Biomech. Eng. 120 (1998) 395–404.
[8] R.F. Difelice, H.H. Bau, Conductive heat transfer between eccentric cylinders with boundary conditions of the third kind, J. Heat Transfer 105 (1983) 678–680.
[9] H.H. Bau, S.S. Sandhal, Heat losses from a fluid flowing in a buried pipe, Int. J. Heat Mass Transfer 25 (1982) 1621–1629.
[10] N.N. Lebedev, I.P. Skalskaya, Y.S. Uflyand, Worked Problems in Applied Mathematics, Dover, 1979.
[11] M.M. Yovanovich, Advanced Heat Conduction, Hemisphere, 1984.
[12] M.R. El-Saden, Heat conduction in an eccentrically hollow, infinitely long cylinder with internal heat generation, J. Heat Transfer 83 (1961) 510–512.
[13] S. Devashish, Development of an improved thermal model to predict in-vivo tissue temperatures, Ph.D. Dissertation, University of Utah (in progress), 2004.
[14] L.X. Xu, K.R. Holmes, B. Moore, M.M. Chen, H. Arkin, Microvascular architecture within the pig kidney cortex, Microvasc. Res. 47 (1994) 293–307.
[15] J.W. Brown, R.V. Churchill, Complex Variables and Applications, McGraw-Hill, Inc., New York, 1996.
[16] G.E. Myers, Analytical Methods in Conduction Heat Transfer, AMCHT Publications, Madison, WI, 1998.
[17] F.P. Incropera, D.P. DeWitt, Fundamentals of Heat and Mass Transfer, John Wiley and Sons, New York, 1996.
[18] E.H. Wissler, An analytical solution countercurrent heat transfer between parallel vessels within a linear axial temperature gradient, J. Biomech. Eng. 110 (1988) 254–256.
[19] J. Landry, N. Marceau, Rate-limiting events in hyperthermic cell killing, Radiat. Res. 75 (1978) 573–585.
[20] M.C. Kolios, M.D. Sherar, J.W. Hunt, Blood flow cooling and ultrasonic lesion formation, Med. Phys. 23 (7) (1996) 1287–1298.
[21] H. Wehner, A.V. Ardenne, S. Kaltofen, Whole-body hyperthermia with water-filtered infrared radiation: technical–physical aspects and clinical experiences, Int. J. Hyperther. 17 (1) (2001) 19–30.
[22] A. Vanne, K. Hynynen, MRI feedback temperature control for the focused ultrasound surgery, Phys. Med. Biol. 48 (2003) 31–43.
[23] A.K. Cousins, On the Nusselt number in heat transfer between multiple parallel blood vessels, J. Biomech. Eng. 119 (1997) 127–129.